JOURNAL OF AIRCRAFT
Vol. 43, No. 3, May–June 2006

Transonic Airfoil Shape Optimization in Preliminary Design Environment

W. Li,* S. Krist,† and R. Campbell‡
NASA Langley Research Center, Hampton, Virginia 23681

A modified profile optimization method using a smoothest shape modification strategy (POSSEM) is developed for airfoil shape optimization in a preliminary design environment. POSSEM is formulated to overcome two technical difficulties frequently encountered when conducting multipoint airfoil optimization within a high-resolution design space: the generation of undesirable optimal airfoil shapes and significant degradation in the off-design performance. To demonstrate the usefulness of POSSEM in a preliminary design environment, a design competition was conducted with the objective of improving a fairly well-designed baseline airfoil at four transonic flight conditions without incurring any off-design performance degradation. Independently, two designs were generated from the inverse design tool CDISC, while a third design was generated from POSSEM using over 200 control points of a cubic B-spline curve representation of the airfoil as design variables for the shape optimization. Pros and cons of all of the airfoil designs are documented along with in-depth analyses of simulation results. The POSSEM design exhibits a fairly smooth curvature and no degradation in the off-design performance. Moreover, it has the lowest average drag at the design conditions among the three airfoil designs, as evaluated from each of three different flow solvers.

Nomenclature

c	=	chord length
c_d	=	drag coefficient
c_l	=	lift coefficient
$c^*_{l,i}$	=	target lift coefficient at the ith design condition
c_m	=	pitching moment
c_p	=	pressure coefficient
$\boldsymbol{D}$	=	vector of airfoil shape parameters
$\mathcal{F}$	=	feasible set of design vectors $\boldsymbol{D}$
$\|f\|_\infty$	=	maximum absolute value of a function $f(t)$ on the interval [0, 1]
$g(t)$	=	parametric form of the y coordinate of the points on an airfoil
M	=	freestream Mach number
r	=	number of design conditions
$\mathcal{S}(\Delta\boldsymbol{D})$	=	smoothness measure of the airfoil modification caused by change of design vector $\Delta\boldsymbol{D}$
t	=	variable of a function defined on the interval [0, 1]
$W^{2,\infty}$	=	Sobolev space of functions with bounded second derivatives
x, y	=	Cartesian coordinates of point on airfoil
α	=	angle of attack
γ_{end}	=	terminal maximum drag-reduction rate
γ_k	=	maximum drag-reduction rate at the kth iteration
γ_0	=	initial maximum drag-reduction rate
Δc_d	=	change in drag coefficient
Δc_l	=	change in lift coefficient
ΔD	=	change of $\boldsymbol{D}$
$\Delta g(t)$	=	parametric form of the y-coordinate change of point on an airfoil
$\Delta g^{(3)}(t)$	=	third derivative of $\Delta g(t)$
$(\Delta g)'(t)$	=	first derivative of $\Delta g(t)$
$(\Delta g)''(t)$	=	second derivative of $\Delta g(t)$
$\Delta\alpha$	=	change of α
δ	=	magnitude of smoothness measure
$\partial c_d/\partial\boldsymbol{D}$	=	gradient of drag coefficient with respect to $\boldsymbol{D}$
$\partial c_d/\partial\alpha$	=	partial derivative of drag coefficient with respect to α
$\partial c_l/\partial\boldsymbol{D}$	=	gradient of lift coefficient with respect to $\boldsymbol{D}$
$\partial c_l/\partial\alpha$	=	partial derivative of lift coefficient with respect to α
ϵ_{ave}	=	average drag reduction at the design conditions
$\epsilon_{\min}$	=	lower bound for acceptable average drag reduction at the design conditions
ρ	=	scaling factor for adjusting the magnitude of smoothness measure
τ_i	=	performance gain factor for the ith design condition

Subscripts and superscripts

i	=	index for the ith design condition
k	=	index of optimization iteration

Presented as Paper 2004-4629 at the AIAA/ISSMO 10th Multidisciplinary Analysis and Optimization Conference, Albany, NY, 30 August–1 September 2004; received 12 October 2004; revision received 17 August 2005; accepted for publication 18 August 2005.

*Senior Research Engineer, Aeronautics Systems Analysis Branch, Systems Analysis Concept Directorate. Member AIAA.

†Aerospace Engineer, Configuration Aerodynamics Branch, Research and Technology Directorate. Member AIAA.

‡Aerospace Engineer, Configuration Aerodynamics Branch, Research and Technology Directorate. Associate Fellow AIAA.

I. Introduction

ENGINEERING design of a complex subsystem (e.g., an airplane wing) consists of three stages: conceptual design (when the wing platform parameters, such as span length, maximum thickness, taper ratio, sweep angle, and aspect ratio, are determined), preliminary design (when the wing shape is determined), and detailed design (when the detailed plan for manufacturing the wing is determined). In a preliminary design environment, designers can quickly identify a fairly good baseline design and then concentrate on improving its performance. In some cases, designers are tasked to improve an existing good design, such as the redesign of a transonic commercial transport, for a few percent performance gain from a more efficient aerodynamic shape.

To demonstrate that an airfoil optimization tool can be truly useful in a preliminary design environment, we must show that the tool can uncover subtle performance gain with nonintuitive shape modifications guided by simulation analysis when started from a fairly good baseline design. Because the baseline is close to an optimal design, it becomes almost impossible to find meaningful performance gain

by searching for an optimal shape in a low-resolution design space (represented by a geometry model with a few shape parameters). An airfoil optimization example was given by Li and Padula[1] to show how performance gain can be adversely affected by low resolution of the design space.

To do aerodynamic shape optimization in a high-resolution design space (represented by a geometry model with many shape parameters), one faces the challenge of how to avoid undesirable oscillatory shapes caused by high frequency components in the parametric geometry model. Earlier attempts to use free-form airfoil shape parameterization (such as curves with 23 sinusoidal basis functions[2] and cubic B-spline curves with 36 control points[3]) led to numerically optimal airfoils with undesirable shapes and oscillatory drag rise curves over a Mach range when multipoint airfoil optimization methods were used. In practice, one could smooth generated optimal airfoil shapes to get rid of undesirable curvature features, but smoothing the shape might nullify some or all of the obtained performance gain. Jameson and his collaborators[4,5] suggested the use of a smoothed gradient of the objective function for shape modification. For constrained optimization, one could project the smoothed gradient into the feasible space. These approaches only address the need for smooth shape modification after the optimization algorithm predicts the best possible shape modification for performance gain. There is no guarantee that the smoothed shape modification is a descent direction for the objective function. In this paper, we propose using the smoothest shape-modification (SSEM) strategy for drag minimization under lift constraints. This method finds the best possible smooth shape modification for performance gain in a Sobolev space[6] that is appropriate for the definition of the gradients of aerodynamic coefficients. (See Ref. 1, Sec. 2 for some explanation on why a Sobolev space is needed for definition of the gradients of aerodynamic coefficients.)

Another challenging issue associated with aerodynamic shape optimization in a high-resolution design space is off-design performance degradation. High-resolution design space allows a multipoint optimization algorithm to exploit the weakness of the optimization formulation because of a lack of information on off-design performance and to trade marginal performance gains at the design conditions with severe off-design performance degradation.[2,7] Petropoulou et al.[8] studied multipoint airfoil optimization with airfoils parameterized by Bezier curves with 34 control points; however, they had no discussion on airfoil curvature oscillation and off-design performance. Recently, Li and Padula[9,10] demonstrated that a robust airfoil optimization method, called the profile optimization method (POM),[7] can find an optimal airfoil with improved performance over a baseline in a range of transonic flight conditions. In particular, the POM was applied to improve the performance of an advanced airfoil used by designers as the baseline airfoil for a transonic wing configuration in a range of Mach numbers.[9] The demonstrated benefit of POM was received by a design team with mixed feelings of excitement and doubt: the optimal airfoil does have 5–10% performance improvement over the baseline in a range of transonic flight conditions, but its curvature profile is too oscillatory. Therefore, the main purpose of this paper is to show that a modified POM using SSEM (called POSSEM) can generate optimal airfoils with fairly smooth curvature and improved performance in a specified range of flight conditions, even though the baseline is well designed for the specified flight conditions and the design space is parameterized by over 200 design variables.

To demonstrate the usefulness of an aerodynamic shape optimization tool (such as POSSEM) in a preliminary design environment, there is one more obstacle to overcome: demonstrating that the tool can generate aerodynamic shapes as good as or better than what the state-of-the-art design process can produce. A state-of-the-art tool for preliminary aerodynamic shape design commonly used at Langley Research Center and in industry is CDISC, developed by Campbell.[11] CDISC is a knowledge-based inverse design tool. In each design cycle, a designer specifies characteristics of a target pressure distribution, and CDISC modifies the current aerodynamic shape iteratively to generate a new shape that has the desired pressure characteristics. For transonic commercial aircraft wing design, the primary goal is to improve the wing performance at the cruise condition(s) without severe penalty at off-design conditions. By trial and error, a designer learns how to achieve performance gains without severe off-design performance degradation and generates an overall best design within the time and resources allocated. It is often impossible to incorporate all of the conflicting design goals and requirements that a designer might consider during the design process into an optimization formulation. Therefore, a practical concern is whether any airfoil optimization method (such as POSSEM), which uses performance information at only a few design conditions, can generate optimal airfoils that are as good as or better than airfoils generated by experienced designers using CDISC.

To address the last concern, we start a design competition with a fairly well-designed supercritical airfoil (denoted by D0) as the baseline airfoil. The objective is to improve the performance of D0 at four transonic flight conditions as much as possible without incurring any undesirable off-design performance degradation or any undesirable shape characteristics. In other words, any candidate airfoil design not only must have good performance when analyzed by flow simulation codes, but also should look like a realistic transonic airfoil.

For the design competition, the first candidate airfoil was generated by using CDISC[11] with MSES[12] for a multipoint design, the second candidate airfoil was designed by using CDISC with OVERFLOW,[13] and the third candidate airfoil was developed through application of the POSSEM method using the adjoint sensitivity information from FUN2D.[14,15] To assess the effect of the different flow solvers on the performance characteristics, each of the three candidate airfoils was analyzed by all three codes. Pros and cons of all of the candidate airfoil designs are documented along with in-depth analyses of simulation results.

The paper is organized as follows. In Sec. II, we introduce a Sobolev space appropriate for variational analysis of the gradients of lift and drag coefficients in two-dimensional transonic viscous flow, and we define a curvature smoothness measure for cubic B-spline parameterization of airfoils that captures both smoothness and magnitude of airfoil shape modification in the Sobolev space. Section III contains a detailed description of POSSEM. In Sec. IV, we document how the baseline airfoil and three candidate airfoil designs are generated for the design competition. Detailed discussions of the performance analysis results for the three airfoil designs are included in Sec. V. The final Sec. VI concludes the paper.

II. Curvature Smoothness Measure for Shape Modification

A key component of POSSEM that differentiates it from POM is use of the SSEM strategy in determining the most appropriate descent direction. In this section, we introduce the curvature smoothness measure, which underlies the SSEM formulation.

It is well known that efficient aerodynamic shapes are smooth. Thus, it is not surprising that airfoil smoothing is a part of many airfoil design or optimization processes. For example, Jameson and coworkers[4,5] used a smoothed gradient to modify the current aerodynamic shape within each optimization iteration, while curvature smoothing is an integral part of CDISC inverse design process. Besides the practical need for smooth aerodynamic shapes, smooth shape modification is necessary to ensure the accuracy of linear Taylor approximations of aerodynamic coefficients[1] because the gradients of aerodynamic coefficients are defined in a Sobolev space.[6] To our knowledge, a precise definition of the appropriate Sobolev space needed for variational analysis of the gradients of lift and drag coefficients in Navier–Stokes flow has yet to be formulated. However, it is known that in subsonic flow change of pressure coefficient is proportional to change of airfoil curvature, which is one rule used in CDISC (see Ref. 11, p. 5). This rule implies that variational analysis of the gradients of lift and drag coefficients with respect to airfoil shape involves the second derivative of the airfoil shape.

Let $y = g(t)(0 \le t \le 1)$ be a parametric representation of the y coordinate of a point on an airfoil. An airfoil shape change can be facilitated by a change in $g(t)$, denoted by $\Delta g(t)$. The important issue is how to measure the "size" of a shape modification represented

by $\Delta g(t)$. From a geometric perspective, $\Delta g(t)$ is considered to be a minor modification if the maximum value of $|\Delta g(t)|$ is small. This definition of size makes sense under visual inspection of the modification to the shape. However, for gradients obtained via variational analysis a small maximum value of $|\Delta g(t)|$ does not imply a small shape modification in the Sobolev space required for the definition of the gradients of aerodynamic coefficients and cannot ensure the accuracy of the linear Taylor approximations of the lift and drag coefficients.[1] Instead, the accuracy of linear Taylor approximations of the lift and drag coefficients depends on the magnitude of the second derivative $(\Delta g)''(t)$ of $\Delta g(t)$. Based on the CDISC rule just mentioned we conjecture that

$$\left.\begin{aligned}\Delta c_l &= \left\langle \frac{\partial c_l}{\partial g}, \Delta g \right\rangle + o(\|\Delta g\|_\infty + \|(\Delta g)''\|_\infty)\\ \Delta c_d &= \left\langle \frac{\partial c_d}{\partial g}, \Delta g \right\rangle + o(\|\Delta g\|_\infty + \|(\Delta g)''\|_\infty)\end{aligned}\right\} \tag{1}$$

where Δc_l and Δc_d denote the actual changes in c_l and c_d as a result of the shape change $\Delta g(t)$; $\partial c_l/\partial g$ and $\partial c_d/\partial g$ denote the gradients of c_l and c_d with respect to the shape change $\Delta g(t)$, respectively; $\langle \cdot, \cdot \rangle$ denotes the value of applying the gradient to a given shape change $\Delta g(t)$; $\|\Delta g\|_\infty$ (or $\|(\Delta g)''\|_\infty$) is the maximum value of $|\Delta g(t)|$ [or $|(\Delta g)''(t)|$] for $0 \le t \le 1$; and the last error term in Eq. (1) satisfies the following condition:

$$\frac{o(\|\Delta g\|_\infty + \|(\Delta g)''\|_\infty)}{\|\Delta g\|_\infty + \|(\Delta g)''\|_\infty}$$

approaches zero as $\|\Delta g\|_\infty + \|(\Delta g)''\|_\infty$ goes to zero.

The expression $\|\Delta g\|_\infty + \|(\Delta g)''\|_\infty$ is called the norm of $\Delta g(t)$ in the Sobolev space $W^{2,\infty}$ (the space of functions with bounded second derivatives). Therefore, to ensure the accuracy of linear Taylor approximations of c_l and c_d, we use a shape modification $\Delta g(t)$ such that $\|\Delta g\|_\infty + \|(\Delta g)''\|_\infty$ is small [i.e., $\Delta g(t)$ has a small norm in $W^{2,\infty}$].

If we use a parametric cubic B-spline representation of an airfoil modification $\Delta g(t)$, then the third derivative $\Delta g^{(3)}(t)$ of the cubic spline $\Delta g(t)$ is a piecewise constant function, that is,

$$\Delta g^{(3)}(t) = v_j \qquad \text{for} \qquad t_{j-1} < t < t_j, \qquad 1 \le j \le n \tag{2}$$

where $0 = t_0 < t_1 < \cdots < t_n = 1$ are the knots of the cubic spline $\Delta g(t)$ and v_j are scalars. Let $\boldsymbol{\Delta D}$ denote the column vector of all B-spline coefficients of $\Delta g(t)$ (i.e., y coordinates of the control points for the B-spline representation of the airfoil modification). Then each v_j is a linear function of $\boldsymbol{\Delta D}$. As a consequence, there is a matrix $\mathcal{S}$ such that the jth component of the matrix-vector product $\mathcal{S}(\boldsymbol{\Delta D})$ is v_j. It follows from Eq. (2) that the maximum value of $|\Delta g^{(3)}(t)|$ is the maximum absolute value of the components of $\mathcal{S}(\boldsymbol{\Delta D})$. Therefore, we can impose an upper bound δ on $|\Delta g^{(3)}(t)|$ by using the following system of linear inequalities:

$$-\delta \le \mathcal{S}(\boldsymbol{\Delta D}) \le \delta \tag{3}$$

which means that each component of the vector $\mathcal{S}(\boldsymbol{\Delta D})$ is bounded below by $-\delta$ and above by δ. If $\delta = 0$, then Eq. (3) forces $\Delta g(t)$ to be a quadratic function of t, resulting in a very smooth but not necessarily small shape modification. Obviously, increasing δ leads to an airfoil shape modification with more oscillatory curvature.

The parameter δ in Eq. (3) not only controls the curvature smoothness of $\Delta g(t)$, but also can be used to control the magnitude of $\Delta g(t)$ in $W^{2,\infty}$, provided that a few standard airfoil geometry constraints are imposed. One standard geometry constraint is to fix the leading-edge (LE) position at $y/c = 0$, that is,

$$\Delta g(t_{\text{LE}}) = 0 \tag{4}$$

where t_{LE} is the parameter value corresponding to the LE. Also, structural requirements lead to thickness constraints at two spar locations:

$$\Delta g(t_1^+) = \Delta g(t_1^-) \qquad \text{and} \qquad \Delta g(t_2^+) = \Delta g(t_2^-) \tag{5}$$

where t_j^+ and t_j^- $(j = 1, 2)$ are parameter values corresponding to two spar locations at the upper and lower surfaces, respectively.

The curvature smoothness constraint (3), together with the three constraints given in Eqs. (4) and (5), ensures that a small δ results in a small shape modification $\Delta g(t)$ in $W^{2,\infty}$. In fact, by Rolle's theorem, Eq. (5) implies that there are two zeros t_1^* and t_2^* of the first derivative of $\Delta g(t)$ [i.e., $(\Delta g)'(t_1^*) = (\Delta g)'(t_2^*) = 0$], which means that there is also a zero t^* of the second derivative of Δg [i.e., $(\Delta g)''(t^*) = 0$]. As a consequence, we have the following estimate for the second derivative of $\Delta g(t)$:

$$|(\Delta g)''(t)| = \left| \int_{t^*}^{t} \Delta g^{(3)}(t)\, \mathrm{d}t \right| \le \left| \int_{t^*}^{t} \left\| \Delta g^{(3)} \right\|_\infty \mathrm{d}t \right| \le \left\| \Delta g^{(3)} \right\|_\infty$$

where $\|\Delta g^{(3)}\|_\infty = \max_{0 \le t \le 1} |\Delta g^{(3)}(t)|$. Similarly, the first derivative of $\Delta g(t)$ can also be bounded above by $\|\Delta g^{(3)}\|_\infty$:

$$|(\Delta g)'(t)| = \left| \int_{t_1^*}^{t} (\Delta g)''(t)\, \mathrm{d}t \right| \le \left| \int_{t_1^*}^{t} \left\| \Delta g^{(3)} \right\|_\infty \mathrm{d}t \right| \le \left\| \Delta g^{(3)} \right\|_\infty$$

Finally,

$$|\Delta g(t)| = \left| \int_{t_{\text{LE}}}^{t} (\Delta g)'(t)\, \mathrm{d}t \right| \le \left| \int_{t_{\text{LE}}}^{t} \left\| \Delta g^{(3)} \right\|_\infty \mathrm{d}t \right| \le \left\| \Delta g^{(3)} \right\|_\infty$$

In other words, with fixed LE and two thickness constraints, decreasing δ in Eq. (3) reduces the Sobolev norm of $\Delta g(t)$ in $W^{2,\infty}$ and, thus, improves the accuracy of the linear Taylor approximations of c_l and c_d. Therefore, we will use Eq. (3) to define the trust regions for airfoil shape optimization. The scalar δ in Eq. (3) controls not only the curvature smoothness of the shape modification, but also the magnitude of the shape modification in $W^{2,\infty}$.

III. Modified Profile Optimization Using Smoothest Shape Modification

Based on parametric cubic B-spline representation of airfoils, SSEM uses the curvature smoothness constraint (3) to define trust regions in a sequential linear-programming method for multi-objective optimization. The trust region defined by Eq. (3) forces the optimization algorithm to find a globally smooth shape modification for performance gain instead of using local shock bumps to improve the performance at a few specified design conditions, even though the latter is the "right" thing to do numerically because of the lack of performance information at off-design conditions.

To describe the airfoil optimization problem, the following notation is introduced. Let $c_{l,i}^*$ be the target lift coefficient at the freestream Mach number M_i for $1 \le i \le r$, and let $\boldsymbol{D}$ be the vector of design variables (such as the y coordinates of the cubic B-spline control points) that defines the airfoil shape. The lift and drag coefficients $c_l(\boldsymbol{D}, \alpha, M)$ and $c_d(\boldsymbol{D}, \alpha, M)$ are functions of the design vector $\boldsymbol{D}$, the freestream Mach number M, and the angle of attack α. With this notation, the multi-objective airfoil optimization problem can be formulated as follows:

$$\left.\begin{aligned}&\min_{D,\alpha_i} \{c_d(\boldsymbol{D}, \alpha_1, M_1), c_d(\boldsymbol{D}, \alpha_2, M_2), \ldots, c_d(\boldsymbol{D}, \alpha_r, M_r)\}\\ &\text{subject to} \quad c_l(\boldsymbol{D}, \alpha_i, M_i) = c_{l,i}^* \ \text{ for } \ 1 \le i \le r \ \text{ and } \ \boldsymbol{D} \in \mathcal{F},\end{aligned}\right\} \tag{6}$$

where $\mathcal{F}$ is the feasible set of airfoil shapes satisfying some geometric constraints (such as fixed LE and thickness constraints).

A standard approach for solving a multi-objective optimization problem is to construct an aggregated objective (such as a weighted average) of all of the objective functions and to find a Pareto solution of the original multi-objective optimization problem by minimizing the aggregated objective function. However, for airfoil shape optimization Drela[2] demonstrated that minimizing a weighted average of drag coefficients at multiple design conditions leads to an optimal

airfoil shape with shock bumps that improve the airfoil performance at the design conditions but cause performance degradation at off-design conditions.

Motivated by POM,[7] we propose to use a design-oriented approach for solving the multi-objective optimization problem. The key idea is to make the optimization algorithm "think" like a designer in search of a Pareto optimal solution. A designer understands that the final design must have good performance over the entire range of flight conditions. By trial and error, the designer adaptively learns how to improve the performance of the current design at one flight condition without adversely degrading the performance at other flight conditions. It is an art accumulated over many years of design experience. A natural question is how a design-oriented optimization method should modify the current design to intelligently mimic the human design process by using the sensitivity information of the objective and constraint functions instead of human experience and knowledge. During the quest for an answer to this question, a sensible conflict-resolution strategy emerged that treats each iteration of multi-objective optimization as optimal decision making with limited information. Note that the optimization method's decision is only based on performance information at a few design conditions (determined by $c^*_{l,i}$ and M_i) without any knowledge of performance at off-design conditions. Therefore, it is nontrivial to determine a shape modification that will not incur off-design performance degradation.

Algorithm for Modified Profile Optimization Using Smoothest Shape Modification (POSSEM)

Let $\boldsymbol{D}^0$ be the initial design vector (i.e., the y coordinates of the control points for the B-spline representation of the initial baseline airfoil). Assume that $\mathcal{F}$ is the set of all design vectors $\boldsymbol{D}$ such that the airfoil corresponding to $\boldsymbol{D}$ has the same thickness as the baseline airfoil at several chord locations (such as the maximum thickness location and two spar locations) and has the same LE as the baseline. Choose the initial and terminal maximum drag-reduction rates γ_0 (with $0.02 \le \gamma_0 \le 0.04$) and $\gamma_{\text{end}} (\approx 0.01)$, respectively, and a lower bound $\epsilon_{\min} (\ge -0.00005)$ for acceptable average drag reduction at the design conditions. Let ρ be a scaling factor (with $0.5 \le \rho < 1$). Then generate a sequence of design vectors $\boldsymbol{D}^{k+1}$ $(k = 0, 1, \ldots)$ as follows.

1) *Compute the initial feasible angles of attack.* Find $\alpha_{1,0}, \alpha_{2,0}, \ldots, \alpha_{r,0}$ such that

$$c_l(\boldsymbol{D}^0, \alpha_{i,0}, M_i) = c^*_{l,i} \qquad \text{for} \qquad 1 \le i \le r$$

2) *Initialize the performance gain factors.* Let $\tau_i = 1$ for $1 \le i \le r$. Initially, assume that the drag at each design condition can be reduced simultaneously by a factor of γ_k. If it does not work, then adaptively decrease one or more of τ_i (in step 4) so that the drag at the ith design condition can be reduced by a factor of $\tau_i \gamma_k$. The use of τ_i allows a cooperative negotiation among the design conditions so that the predicted drag-reduction rate at one design condition is exactly γ_k while the predicted drag-reduction rates at other design conditions could be fractions of γ_k (but no predicted performance loss is allowed at any design condition).

3) *Solve a trust-region subproblem.* Let $c_{d,i,k}$ and $c_{l,i,k}$ be the linear Taylor approximations of the drag and lift coefficients at $(\boldsymbol{D}^k, \alpha_{i,k}, M_i)$:

$$c_{l,i,k}(\Delta \boldsymbol{D}, \Delta\alpha_i) = c_l\left(\boldsymbol{D}^k, \alpha_{i,k}, M_i\right) + \left\langle \frac{\partial c_l}{\partial \boldsymbol{D}}, \Delta \boldsymbol{D} \right\rangle + \frac{\partial c_l}{\partial \alpha} \Delta\alpha_i$$

$$c_{d,i,k}(\Delta \boldsymbol{D}, \Delta\alpha_i) = c_d\left(\boldsymbol{D}^k, \alpha_{i,k}, M_i\right) + \left\langle \frac{\partial c_d}{\partial \boldsymbol{D}}, \boldsymbol{\Delta D} \right\rangle + \frac{\partial c_d}{\partial \alpha} \Delta\alpha_i$$

where all of the derivatives are evaluated at $(\boldsymbol{D}^k, \alpha_{i,k}, M_i)$, and $\langle \cdot, \cdot \rangle$ denotes the dot product of vectors. Consider the following trust-region subproblem for Eq. (6):

$$\left.\begin{array}{ll} \max_{\Delta D, \Delta\alpha_i} \quad \gamma \quad \text{such that} & \\ \boldsymbol{D}^k + \Delta \boldsymbol{D} \in \mathcal{F}, \qquad -\delta_k \le \mathcal{S}(\Delta \boldsymbol{D}) \le \delta_k & \\ \alpha_{\min} - \alpha_{i,k} \le \Delta\alpha_i \le \alpha_{\max} - \alpha_{i,k} \qquad \text{for} \qquad 1 \le i \le r & \\ c_{l,i,k}(\Delta \boldsymbol{D}, \Delta\alpha_i) = c^*_{l,i} \qquad \text{for} \qquad 1 \le i \le r & \\ c_{d,i,k}(\Delta \boldsymbol{D}, \Delta\alpha_i) \le (1 - \tau_i \gamma) \cdot c_d\left(\boldsymbol{D}^k, \alpha_{i,k}, M_i\right) & \\ \qquad\qquad \text{for} \qquad 1 \le i \le r & \end{array}\right\} \quad (7)$$

If the optimal objective function value γ^* of Eq. (7) is zero, then $\boldsymbol{D}^k$ is a Pareto optimal solution and terminates the iteration with $\boldsymbol{D}^k$ as the output. Otherwise, the optimal objective function value γ^* of Eq. (7) gives a reduction of the linearized drag at the ith design condition by at least a factor of $\tau_i \gamma^*$. Choose $\delta_k > 0$ such that the optimal objective function value of Eq. (7) is exactly γ_k. Let $(\Delta \boldsymbol{D}^k, \Delta\alpha_{1,k}, \ldots, \Delta\alpha_{r,k})$ be the least norm solution of Eq. (7).

4) *Adjust the performance gain factors if necessary.* Compute the predicted drag-reduction rate at each of the design conditions:

$$\gamma_{i,k} = \frac{c_{d,i,k}\left(\Delta \boldsymbol{D}^k, \Delta\alpha_{i,k}\right) - c_d\left(\boldsymbol{D}^k, \alpha_{i,k}, M_i\right)}{c_d\left(\boldsymbol{D}^k, \alpha_{i,k}, M_i\right)} \quad \text{for} \quad 1 \le i \le r$$

If $\max\{\gamma_{1,k}, \gamma_{2,k}, \ldots, \gamma_{r,k}\} > \gamma_k$ (which implies that the trust-region size δ_k is too large for the required maximum drag reduction), find the smallest index j such that $\gamma_{j,k} = \tau_j \gamma_k$ and $\tau_j = \max\{\tau_1, \tau_2, \ldots, \tau_r\}$. Replace τ_j by $\tau_j/2$, and go back to step 3.

5) *Generate the new iterate.* Define $\boldsymbol{D}^{k+1} = \boldsymbol{D}^k + \Delta \boldsymbol{D}^k$.

6) *Find the feasible angles of attack for* $\boldsymbol{D}^{k+1}$. Use $\alpha_{i,k} + \Delta\alpha_{i,k}$ as the initial guess to find $\alpha_{i,k+1}$ such that $c_l(\boldsymbol{D}^{k+1}, \alpha_{i,k+1}, M_i) = c^*_{l,i}$ for $1 \le i \le r$.

7) *Decide whether the new iterate can be accepted.* Compute the actual average drag reduction ϵ_{ave} at the design conditions:

$$\epsilon_{\text{ave}} = \frac{1}{r}\left[\sum_{i=1}^{r} c_d\left(\boldsymbol{D}^{k+1}, \alpha_{i,k+1}, M_i\right) - \sum_{i=1}^{r} c_d\left(\boldsymbol{D}^k, \alpha_{i,k}, M_i\right)\right]$$

Reset the maximum drag-reduction rate as follows:

$$\gamma_{k+1} = \begin{cases} \gamma_k, & \text{if} \quad \epsilon_{\text{ave}} > \epsilon_{\min} \quad \text{and} \quad \gamma_k = \gamma_0 \\ \gamma_k, & \text{if} \quad \epsilon_{\min} < \epsilon_{\text{ave}} < 0.0001 \\ \gamma_k/\rho, & \text{if} \quad \epsilon_{\text{ave}} \ge 0.0001 \quad \text{and} \quad \gamma_k < \gamma_0 \end{cases}$$

If $\epsilon_{\text{ave}} > \epsilon_{\min}$, update k by $k+1$, and go back to step 2.

8) *Decide whether the iteration should be terminated.* If $\gamma_k = \gamma_{\text{end}}$, terminate the iteration, and choose the best overall design among $\boldsymbol{D}^1, \ldots, \boldsymbol{D}^k$; otherwise, replace γ_k by $\max\{\rho\gamma_k, \gamma_{\text{end}}\}$, and go back to step 2.

SSEM refers to finding the smallest δ_k such that the optimal objective function value of Eq. (7) is γ_k. In nontechnical terms, SSEM searches for the smoothest shape modification among all possible shape modifications that achieve the given drag-reduction rate γ_k, as predicted by linear approximations of the (nonlinear) lift and drag coefficients, at the design conditions. As the current configuration moves closer to a (locally) Pareto optimal shape for the given design conditions, it becomes more difficult to find a smooth shape modification that leads to a configuration with the same rate of performance gain at all of the design conditions. In such a case, it is necessary to use the performance gain factors τ_i for facilitating inhomogeneous performance gains at different design conditions. The rationale behind the adjustment of τ_i is the following. For the smallest δ_k that allows the required drag-reduction rate of at least $\tau_i \gamma_k$ at the ith design condition for $1 \le i \le r$, one of the predicted drag-reduction rates $\gamma_{i,k}$ might be larger than γ_k. In such a case, we find an index j such that the drag reduction by a factor of $\tau_j \gamma_k$ at the jth design condition contributes to the requirement of a larger δ_k than necessary for the drag reduction by a factor of γ_k at another design condition. By reducing the requirement for predicted drag-reduction rate at the jth design condition, we try to find the right trust-region size δ_k such that the drag-reduction rate for one design

condition is γ_k, while the drag-reduction rates for the other design conditions are as close to γ_k as possible. The performance gain factors τ_i allow adaptive adjustment of the predicted drag-reduction rate at each design condition so that POSSEM can optimally balance the needs for performance gains at different design conditions and resolve potentially conflicting demands of the resource (the size of δ_k) by the design conditions.

Note that unless D^k is a Pareto optimal solution of Eq. (6), step 3 of POSSEM always generates a solution. As long as the average drag reduction at all of the design conditions is acceptable (i.e., $\epsilon_{\text{ave}} > \epsilon_{\min}$), we accept D^{k+1} as the new iterate. This strategy is different from minimizing the weighted sum of drag at the design conditions because the latter might intentionally seek a good performance gain at one design condition with performance loss at another design condition. For POSSEM, performance loss at a design condition occurs only when the linear prediction of drag reduction cannot be realized because of approximation errors, which can be significant when δ_k is too large or $\tau_i \gamma_k$ is too small.

The termination criterion given in POSSEM is not a mathematical one; instead, it is a heuristic rule. A small negative value of $\epsilon_{\min}$ tolerates a marginal degradation of the performance at the design conditions. This mechanism allows POSSEM to "escape" from a local Pareto solution and explore other potential solutions. The rule for updating the maximum drag reduction rate γ_k is also based on our experience in transonic airfoil shape optimization, but it can easily be reformulated by using other rules.

The SSEM not only makes the predicted performance gains more realizable, but also finds a favorable global shape modification that improves the performance over the range of design conditions, instead of creating local curvature bumps for airfoil performance gains at just the specified design conditions.

POSSEM is significantly different from the smoothed gradient method used by Jameson and his collaborators.[4,5] The smoothness of the shape modification in POSSEM is adaptively changing from a very smooth shape modification initially to relatively smooth shape modification as the design moves closer to a locally Pareto optimal airfoil. Moreover, the smoothest shape modification in POSSEM always provides performance gains based on linear predictions of the lift and drag. For the smoothed gradient method, the separation between smoothing and selection of a descent direction makes it difficult to know how much smoothing should be applied or whether a smooth shape modification for performance gain is possible if the smoothed gradient fails to yield a performance gain.

IV. Design Competition

Modern commercial transonic wings are quite efficient, making it difficult to extract aerodynamic performance gains of much more than a few percent in typical industrial preliminary design studies. In contrast, the literature is replete with examples of aerodynamic optimization results showing dramatic performance improvements, with some as large as 50%. In fact, there have been instances in which the utility of a design method has been obscured by invocation of the "start with a dog" principle in design method promotion, wherein any design method can be shown to provide dramatic performance improvements provided that the baseline configuration is sufficiently inappropriate for the application at hand. To preclude the possibility of exaggerating the capabilities of POSSEM or overlooking its limitations, a design competition was conducted with each of the authors working independently to develop an airfoil design starting from a fairly well-designed baseline. The first author utilized POSSEM, whereas the last two authors employed the CDISC inverse design method.

A complicating aspect of the design competition is that the three designs were generated by using three different flow solvers. The decision to use different solvers was based primarily on convenience for the designers, allowing them to use the tools with which they were most familiar and thereby minimize the effort required to complete the work. Another advantage of this approach is that some insight into how flow solver differences impact the characteristics of the designs is obtained, providing a measure of how robust the design approaches are across tools with differences in solution fidelity. Of course the disadvantage is that application of the design procedures within the framework of a single flow solver would have provided a much more direct comparison of design method effectiveness. Regardless of any deficiencies, the selected approach is in fact representative of collaborative design efforts involving multiple teams each using their preferred tool set.

The first code, MSES,[12] is a coupled Euler/boundary-layer method that provides very rapid turnaround, making it particularly suitable for use in the early stages of preliminary design. The other two codes, OVERFLOW[13] and FUN2D,[14,15] are Navier–Stokes flow solvers that use overset structured grids and unstructured grids, respectively. These codes, which include a higher level of flow physics and require considerably more time to run than MSES, would typically be used to fine tune airfoil designs. This level of flow physics would also be consistent with that used to evaluate the final three-dimensional configuration with the airfoil integrated into the wing.

For the design competition, the first candidate airfoil was generated by using CDISC with MSES for a multipoint design, the second candidate airfoil was designed by using CDISC with OVERFLOW, and the third candidate airfoil was developed through application of the POSSEM method using the adjoint sensitivity information from FUN2D. Both OVERFLOW and FUN2D were run using the Spalart–Almaras one-equation turbulence model. To assess any effect of the different flow solvers on the performance characteristics, each of the three candidate airfoils was analyzed by all three codes.

The goal for the design competition is to reduce the average drag at the following four design conditions without any off-design performance degradation: $M_1 = 0.7$ and $c^*_{l,1} = 0.7$, $M_2 = M_3 = M_4 = 0.76$ with $c^*_{l,2} = 0.76$, $c^*_{l,3} = 0.64$, and $c^*_{l,4} = 0.70$. The Reynolds number for viscous flow simulations is 30×10^6. The design conditions are representative of those used in industrial applications, with the first condition used to prevent degradation in the climbout performance and the remaining three conditions used to ensure suitable performance over the range of lift coefficients to be experienced at the design cruise speed ($M = 0.76$). Note that the goal for the design competition is only qualitative in terms of off-design performance degradation; further discussion of what exactly that implies is saved until later in the evaluation of the candidate airfoil designs.

The design of the baseline airfoil D0 was initiated from a seed airfoil extracted from a modern transport configuration by using CDISC coupled with MSES. To maintain consistency with supercritical airfoil design rules for the midcruise condition of ($M = 0.76$, $c_l = 0.7$), this seed airfoil was thickened slightly to give a maximum thickness of 12%. The CDISC flow constraint for "optimum rooftop," which automatically determines shock location and the shape of the supersonic rooftop pressure coefficient distribution, was selected to reduce the wave drag. In an attempt to get good performance over the range of cruise lift coefficients, we decided to design at the lowest value ($c_l = 0.64$) using the maximum allowable compression of the supercritical flow. A flow constraint that maintains the original pitching moment was also applied. In addition to these flow constraints, a geometry constraint that enforces an effective airfoil thickness based on maximum skin stress between two spar locations was used to maintain the effective thickness of the original airfoil. This constraint meets the structural requirement while allowing more design freedom than fixed spar depth constraints.

The new airfoil from this design had significantly better performance than the original seed airfoil. The average drag at the four design conditions for the new airfoil was 22 counts (i.e., 0.0022 in c_d value) less than the original in spite of being 17 counts worse at ($M = 0.70$, $c_l = 0.70$). In an effort to improve the performance at the low Mach design condition, the new design was blended with the original geometry to produce an airfoil that had equal drag values at $M = 0.70$ and 0.76 for $c_l = 0.70$. This blending raised the average drag about one count relative to the initial design but was thought to give better overall performance for the entire range of (M, c_l) being considered. However, CDISC's smoothing still leaves the blended airfoil with some minor curvature oscillation, resulting in a cubic B-spline interpolation of the airfoil data that has an oscillatory curvature profile. Thus, we apply CFACS (a spline-based airfoil curvature

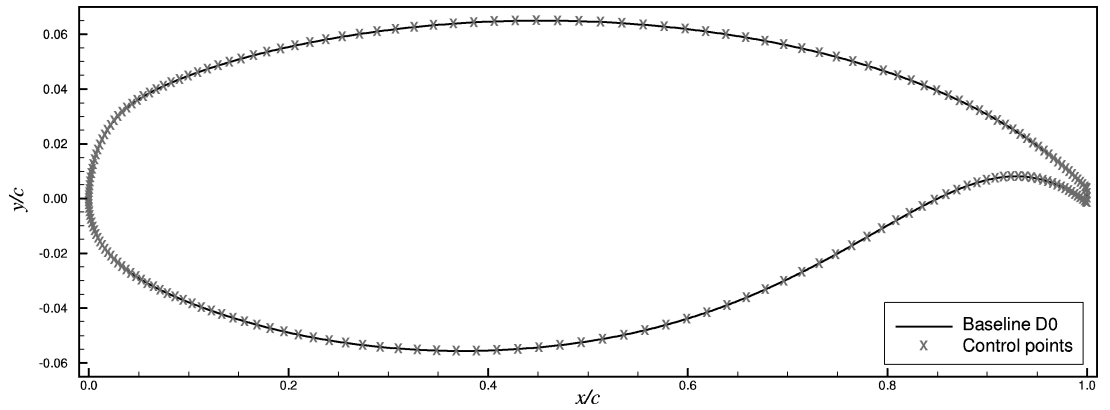

Fig. 1 Shape of baseline D0 and 206 control points for cubic B-spline representation of D0.

smoothing code)[16] to get rid of the minor curvature oscillation with insignificant geometry modification. The resulting airfoil, denoted as D0, has smooth curvature with identical performance characteristics as the blended airfoil. The shape of D0 is defined by 101 grid points on the upper surface and 101 grid points on the lower surface. See Fig. 1 for the airfoil shape represented by the B-spline interpolation of the grid points.

Although the approach used to design D0 was selected to give good multipoint performance, it was still basically a single-point design in that no CDISC design was done at $M = 0.70$. In an attempt to further improve upon this case, a dual-point design was carried out with CDISC/MSES starting from D0. The first design was done at the midcruise condition ($M = 0.76$, $c_l = 0.70$) using the optimum rooftop constraint at 80% of the maximum compression and relaxing the pitching moment constraint to permit a slightly more nose down value. The second design was at ($M = 0.70$, $c_l = 0.76$), with the higher c_l value chosen because the shocks at the lower lift design conditions were already fairly weak. The full maximum compression value was used for this case, and the pitching moment was not constrained. The effective thickness constraint was used in both design cases, and additional geometry smoothing was employed at the second design case to minimize any local curvature bumps that might be generated in weakening the shock near the leading edge.

As with D0, these two airfoil designs were then blended in a proportion that gave about the same drag values at $M = 0.70$ and $M = 0.76$ for $c_l = 0.70$. The resulting airfoil, designated as D1, has an average drag improvement of about three counts relative to D0. Although this dual-point design approach is fairly simplistic, it did result in a noteworthy improvement in performance relative to a refined initial airfoil.

Although the strategy employed to design D1 can be characterized as a turn-the-crank approach to dual-point design, the strategy utilized in generating D2 is one of obstinate persistence. Airfoil D2 was generated by using OVERDISC, which couples CDISC to the OVERFLOW Navier–Stokes code for overset grids. As such, thickness constraints are the same as those applied to D1; however, pitching moment was unconstrained.

The strategy for this design was to perform sequential parametric variations of variables in the CDISC flow constraints. For example, for the CDISC constraint "polynomial rooftop," which was used to define the characteristics of the supercritical rooftop and shock location, four variables are used to specify the position of the leading edge peak of the rooftop, the change in c_p from the peak to the shock, the chordwise position of the shock, and an exponent defining the polynomial shape of the rooftop. Hence, the first five intermediate designs started from D0 and assessed the effect of varying the change in c_p from the peak to the shock. Upon selection of the best setting for this variable, the next three intermediate designs assessed the effect of varying the chordwise location of the shock, again starting from D0. This process was continued for all remaining variables in the polynomial rooftop constraint and the variables in two other constraints, one on the airfoil curvature and another on the characteristics of the lower surface-pressure coefficient distribution. In addition, selected intermediate designs were smoothed by using CFACS and were reevaluated to assess the multipoint design benefits of smoothing. In all, 35 intermediate designs were generated in developing the final shape of D2.

Although technically a single-point design in that target pressure distributions were developed for and applied at the design condition of ($M = 0.76$, $c_l = 0.76$), each design was analyzed at the other three design conditions. Decisions as to which intermediate designs gave the best result were based on the maximum lift-to-drag ratio (L/D) value at $M = 0.76$ (which usually occurred at $c_l = 0.70$), balancing L/D to be roughly equivalent at $c_l = 0.76$ and $c_l = 0.64$ for $M = 0.76$, and maintaining lower drag at ($M = 0.70$, $c_l = 0.70$) than at ($M = 0.76$, $c_l = 0.70$).

POSSEM uses FUN2D to compute the aerodynamic coefficients and their derivatives with respect to α and the control points of a cubic B-spline representation of the airfoil shape. To set up the problem for FUN2D evaluation of the derivatives of c_l and c_d, we first compute the cubic B-spline interpolation of the airfoil data points with the centripetal parameterization. The resulting B-spline curve has 206 control points, with four control points to specify the vertical line segment at the trailing edge (TE) (see Fig. 1).

The design vector $\boldsymbol{D}$ consists of 206 y coordinates of the control points of a cubic B-spline curve that represents an airfoil. The feasible set $\mathcal{F}$ consists of $\boldsymbol{D}$, which has a corresponding airfoil that satisfies the following three conditions: 1) the airfoil has the same thickness as D0 at the chord locations $x/c = 0.15$, 0.4, 0.6, and 0.95; 2) the vertical line segment at the TE of the airfoil has the same length as that of D0; and 3) the airfoil has the same LE as D0. Chord location $x/c = 0.4$ is the maximum thickness (12%) location of D0, while $x/c = 0.15$ and $x/c = 0.6$ are spar locations. Fixing the LE point avoids potentially unnecessary vertical shifting of the airfoil by POSSEM. The first three thickness constraints are from structural requirements. The thickness constraint at $x/c = 0.95$ ensures that the airfoil does not become too thin near the TE because a thin TE segment leads to structural weakness near the TE. For the same reason, we do not want to reduce the length of the vertical line segment at the TE. Note that the thickness constraints used by POSSEM are much more restrictive than the constraint on effective thickness of the airfoil. Because D0 is a fairly well-designed airfoil, we set $\gamma_0 = 2\%$, $\gamma_{\text{end}} = 1\%$, $\rho = 0.5$, and $\epsilon_{\min} = -0.00005$ in POSSEM to generate D3.

One might think that it is unnecessary to use so many design variables for airfoil shape optimization. However, another run of POSSEM with 249 control points, rather than the 206 for D3, yields an optimal airfoil with 0.7 count less average drag at the design conditions than D3 (using FUN2D analysis).

Although D1 and D3 were generated automatically, D2 was designed by a labor-intensive, interactive process. A standard two-point inverse design process produced D1 within 30 min on a single-processor computer. POSSEM found the optimal solution D3 in

about 34 h of wall time using a linux cluster of eight processors, after 16 optimization iterations. Even though each design cycle for D2 only required about 2h of computer time on a single processor, it took two weeks to generate D2 with 37 design cycles. The delay was mainly because of the interactive nature of the design process.

V. Evaluation of Candidate Airfoil Designs

To ensure consistency in the analyses of the three designs with the three different codes, the same grid-point distribution, with 241 grid points on the airfoil surface, is used to generate the computational grids. The grids used in the CDISC inverse design of D1 and D2 embody the same characteristics as the analysis grids, but POSSEM uses a grid with 405 grid points on the airfoil surface for the FUN2D-based optimization. That is, the grid used to generate D3 with POSSEM is quite different from the grid used for evaluation of D3.

Pressure distributions for the baseline and three designs at the three design conditions for the cruise speed $M = 0.76$, as computed from the codes used to construct the designs, are shown in Fig. 2. In the plot for $c_l = 0.76$, all three designs position the shock at roughly 60% of chord. This result is a little surprising because D1 uses the CDISC constraint for optimum rooftop to automatically determine the rooftop shape and shock position at ($M = 0.76$, $c_l = 0.70$), D2 uses the CDISC constraint for polynomial rooftop to explicitly set the shock location based on results from a parametric study of designs at ($M = 0.76$, $c_l = 0.76$) with evaluation of the resulting airfoils at the other three conditions, and the shock position of D3 results from complex trades within the optimization procedure. There is little to distinguish between the rooftops of D2 and D3, with D3 being more oscillatory with slightly more leading-edge suction and a stronger compression after the leading-edge peak. The rooftop of D1 is elevated above those of D2 and D3 with a much crisper shock and stronger aft shock compression; as is shown presently, these differences are primarily caused by differences in the codes. On the lower surface, all three designs generate a stronger aft loading. However, in what is the most unexpected difference between the designs D3 also generates more forward loading with less midspan loading.

The pressure distributions at $c_l = 0.70$ show similar trends, with the shock position for D1 slightly forward of that for D2. However, D3 has an extremely smooth rooftop and is essentially shock free. Conversely, at $c_l = 0.64$ the rooftop of D3 is quite oscillatory with a strong aft shock, while D2 exhibits a fairly flat midspan rooftop and D1 is essentially shock free with some wobbles.

Differences in the characteristics of the designs caused by the different codes used in generating them are illustrated in Fig. 3, which shows pressure distributions at ($M = 0.76$, $c_l = 0.70$) for each design as computed from each of the three codes. Differences in the lower surface-pressure distributions computed from the three codes are insignificant. On the upper surface, the largest difference between the codes is that MSES predicts a more forward, sharper shock with a stronger aft shock compression for each of the three designs, thereby providing an explanation of the apparent elevated rooftop level of D1 in Fig. 2. Upper surface-pressure distributions from OVERFLOW and FUN2D are in fairly close agreement; the D1 shock position from FUN2D is slightly aft of that from OVERFLOW, whereas for D2 and D3, FUN2D predicts shock-free behavior while OVERFLOW predicts a mild shock at this condition. Particularly noteworthy is that differences in the shock position and rooftop levels between MSES and OVERFLOW are the largest for D1 and smallest for D3, suggesting that D3 is the least sensitive to code differences among the three designs. The question as to whether the relative sensitivity of D1 and insensitivity of D3 to code differences is caused by differences in design strategies or differences in the codes with which they were designed remains unresolved at this time.

The surface shape and upper surface curvature for the baseline and three designs are shown in Fig. 4. The surface shapes, which are

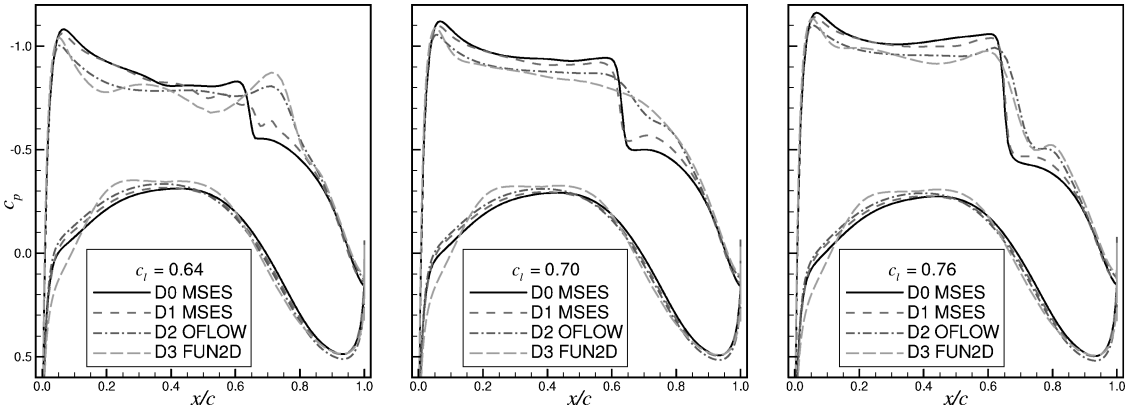

Fig. 2 Pressure coefficient distributions of the baseline and three designs at $M = 0.76$ for $c_l = 0.64$, 0.70, and 0.76, from the codes used for each design; MSES for D0 and D1; OVERFLOW for D2; and FUN2D for D3.

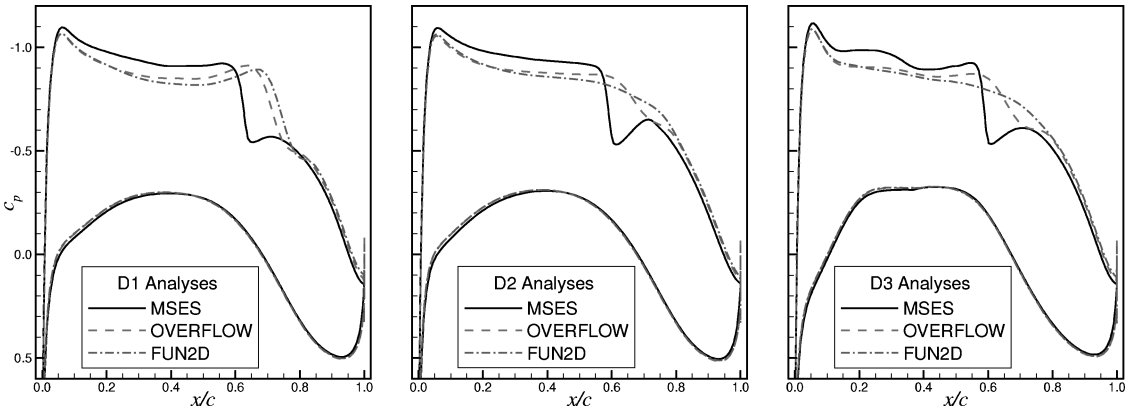

Fig. 3 Pressure coefficient distributions of the three designs computed by FUN2D, MSES, and OVERFLOW at ($M = 0.76$, $c_l = 0.70$).

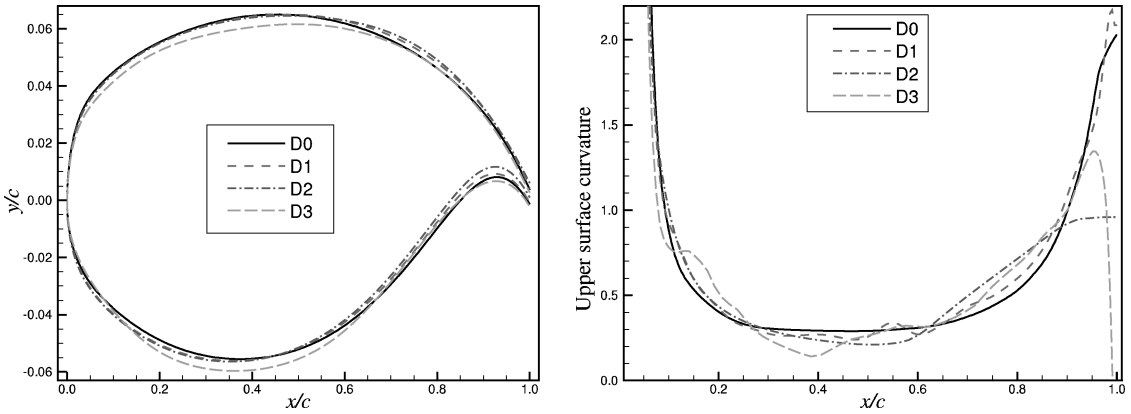

Fig. 4 Airfoil shape and upper surface curvature for the baseline D0 and three designs D1, D2, and D3.

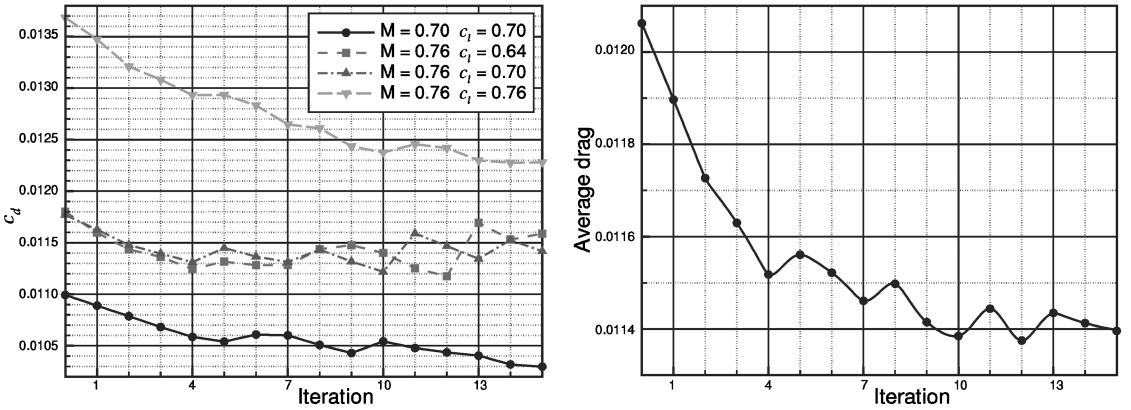

Fig. 5 Drag history and average drag history from POSSEM with D3 as the 10th iterate.

plotted with the leading edge of each airfoil at $y/c = 0.0$, indicate that the change in incidence from the baseline is largest for D2 (a decrease) and smallest for D3 (a slight increase). Plots of the thickness (not shown) indicate that D1 and D2 both increase the thickness of the forward spar by roughly 2% and decrease the thickness of the aft spar by roughly 0.8% with D2 showing a slight reduction in the maximum thickness (less than 0.1%), while D3 preserves the thickness at both spars and the maximum thickness. As just noted, these differences are caused by the use of different thickness constraints within CDISC and POSSEM. Plots of the camber (also not shown) indicate decreases in the camber of D1 and D2 over the forward 50% of chord by as much as 45% with increases in camber over the aft end, while D3 decreases the camber over the first 70% of chord by as much as 120% while essentially maintaining the aft camber.

The curvature plot shows a close-up of the detail of the upper surface curvature because that is the area where severe oscillations are frequently generated in multipoint optimizations of transonic airfoils. The curvature profiles of the baseline and D2 are extremely smooth, as both designs were run through the airfoil curvature smoothing code CFACS. D1 is also fairly smooth owing to the smoothing invoked within the CDISC design process; the minor oscillations, particularly at $x/c = 0.55$, are generated during the procedure used to blend the point designs for flight conditions ($M = 0.70$, $c_l = 0.76$) and ($M = 0.76$, $c_l = 0.70$), respectively. Airfoil D3 is the least smooth of the designs, with notable curvature oscillations at $x/c = 0.1$ and 0.4; nevertheless, its curvature is considerably smoother than that seen with more conventional multipoint optimizations. Also, the curvature of D3 at the trailing edge decreases sharply, with the upper surface shape at the tip of the trailing edge becoming convex rather than concave, while the trailing-edge curvature for D2, which is half the magnitude of that for the baseline and D1, was explicitly designed into the shape using a curvature constraint within CDISC.

Of particular interest in evaluating the behavior of POSSEM is that, although its formulation is based on the SSEM, D3 still embodies some notable curvature oscillations. This behavior can be explained, or perhaps rationalized, by considering both the drag history and upper surface curvature profiles at intermediate iterations, as shown in Figs. 5 and 6. The drag history in Fig. 5 indicates a steady decline in drag at all four design conditions through iteration 4. Beyond that, there is a fairly steady decline in drag at ($M = 0.76$, $c_l = 0.76$) and to a lesser extent at ($M = 0.70$, $c_l = 0.70$), but the drag at ($M = 0.76$, $c_l = 0.64$) and ($M = 0.76$, $c_l = 0.70$) more or less oscillates about some mean value. Likewise, the curvature of the intermediate designs is smooth through iteration 4, after which oscillations begin to appear and continue to grow with further iterations (see Fig. 6). Hence, as the later iterations proceed and POSSEM tries to harvest subtle performance gains, it is forced to use a relatively large δ_k for the shape modification, which in turn introduces curvature oscillations. Clearly, after iteration 4 POSSEM cannot find a smooth shape modification that would improve the performance for at least one design condition while maintaining the performance at other design conditions. The average drag-reduction tolerance $\epsilon_{\min} = -0.00005$ allows POSSEM to accept a minor performance loss at iteration 5 in hope of "escaping" the current local Pareto solution. Over the next two iterations, POSSEM was able to find iterate 7 that has lower drag at ($M = 0.76$, $c_l = 0.76$) than iterate 4 and maintains the same performance as iterate 4 at the other design conditions.

Note that iterates 4 and 7 have almost identical shapes, but iterate 7 has more oscillatory upper surface curvature (see Fig. 6), suggesting that POSSEM was searching for places on the airfoil surface to put minor curvature oscillations for reducing the shock strength at ($M = 0.76$, $c_l = 0.76$), with no adverse effects on performance at the other design conditions. If such a strategy is deemed undesirable, then one could set $\epsilon_{\min} = 0$ (i.e., not accepting any average

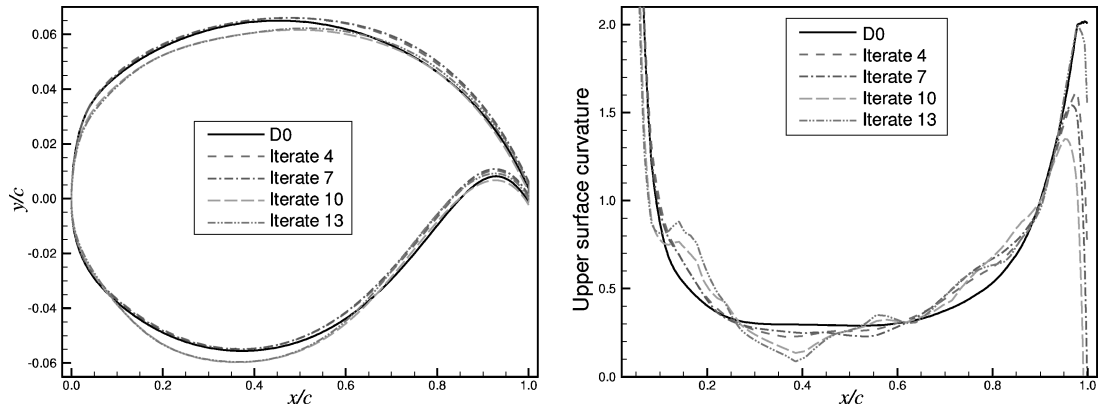

Fig. 6 Airfoil shapes and their upper surface curvature profiles from POSSEM at intermediate iterates.

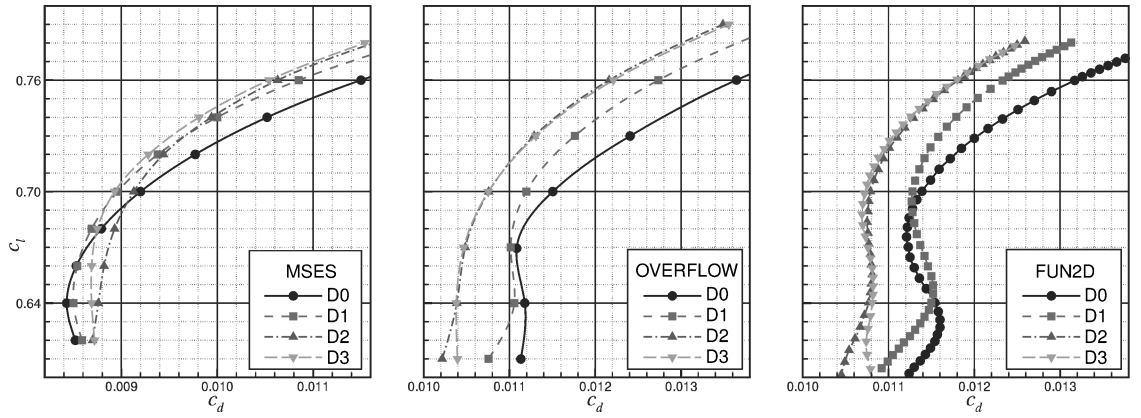

Fig. 7 Drag polars of the baseline D0 and three designs D1, D2, and D3 at $M = 0.76$ as computed from MSES, OVERFLOW, and FUN2D.

performance loss) and terminate POSSEM after iteration 4. A total of about 0.75 counts of average drag reduction was accumulated during the three iterations after iteration 7 (see Fig. 5), which along with the large difference between iterate 7 and iterate 10 (see Fig. 6) attests to the fact that POSSEM was using unreliable linear predictions of the aerodynamic coefficients (caused in part by large δ_k) to search for marginal performance improvement. As a result, curvature oscillations of the airfoil shape increase dramatically during these three iterations. Moreover, once curvature oscillations exist in the shape, POSSEM does not have the capability to take them out (which is precisely why the baseline definition embodies an airfoil that has been smoothed with CFACS). Also of interest is that the major change in camber occurs between iteration 7 and iteration 10, while the sharp reduction in trailing-edge curvature happens between iterations 10 and 13. Iterate 12 has a negligibly better overall performance at the design conditions than iterate 10, with performance trades among the design conditions. The choice of iterate 10 instead of iterate 12 as D3 is caused by the better performance of iterate 10 at the midcruise condition of ($M = 0.76$, $c_l = 0.70$).

We begin the discussion on the performance of the three designs by considering the drag polars at $M = 0.76$ for each of the designs as computed by each of the codes, which are shown in Fig. 7. Differences in absolute drag levels (about 0.0020 in c_d) between MSES and the two Navier–Stokes codes are quite large, with MSES levels on the order of 20 counts lower. Differences between drag levels from OVERFLOW and FUN2D are more subtle, with FUN2D exhibiting larger drag levels at lower lift coefficients and smaller drag levels at higher lift coefficients. Hence, whereas FUN2D predicts larger drag levels at $c_l = 0.64$ than at $c_l = 0.70$ for D0, D1, and D3, both MSES and OVERFLOW indicate that the drag at $c_l = 0.64$ is lower than that at $c_l = 0.70$ for all four designs.

The expectation going into this multicode design effort was that the design from each code would be the best performer within that code, which is quite common in a simulation-based collaborative design environment. The drag polar confirms this expectation for the CDISC-generated designs. Within MSES, D1 substantially outperforms D2 except at the highest lift levels, whereas within OVERFLOW, D2 substantially outperforms D1 everywhere. Somewhat surprising, though, is that the performance of D3 is competitive with D1 in MSES, having higher drag at low lift levels balanced by lower drag at high lift levels, while exhibiting virtually identical performance to D2 within OVERFLOW. Within FUN2D, the performance of D3 is marginally better than that of D2 except below $c_l = 0.64$ and much better than that of D1 everywhere.

A somewhat different perspective on the performance of the three designs can be gleaned from plots of the lift-to-drag ratio, as shown in Fig. 8. Here the MSES results indicate that the maximum L/D values for D1 and D3 are almost the same, with the D3 curve essentially representing a shift to higher c_l levels, while the maximum L/D value for D2 is substantially lower than that of the baseline as well as D1 and D3. Differences in the curves between OVERFLOW and FUN2D primarily lie in the fact the maximum L/D values for all three designs lie around $c_l = 0.70$ in OVERFLOW and $c_l = 0.73$ in FUN2D.

The relatively poor performance of D2 within MSES and D1 within OVERFLOW and FUN2D can be explained in part by examining once again the pressure distributions. Pressure distributions from MSES for the three designs at the three design conditions with $M = 0.76$ are shown in Fig. 9. At $c_l = 0.64$, D1 is essentially shock free while both D2 and D3 exhibit a double shock and the elevated drag levels associated with this feature. Conversely, at $c_l = 0.76$ the shock is located at roughly the same position for all three designs, but a stronger shock, hence greater drag, is exhibited by D1. The situation at $c_l = 0.70$ is less obvious, as the pressure distributions for D2 and D3 are quite similar with the shock located forward of that for D1, while the shock strengths for all three designs are roughly

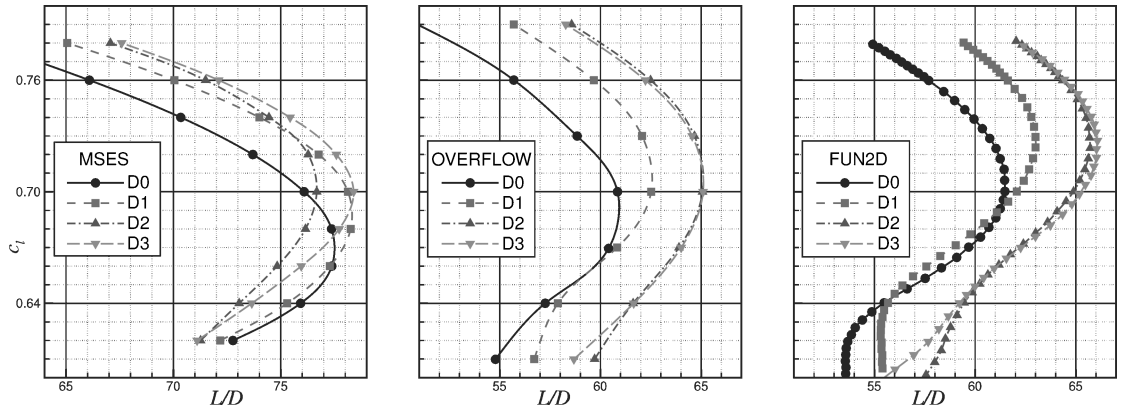

Fig. 8 Lift-to-drag ratio of the baseline D0 and three designs D1, D2, and D3 at $M = 0.76$ as computed from MSES, OVERFLOW, and FUN2D.

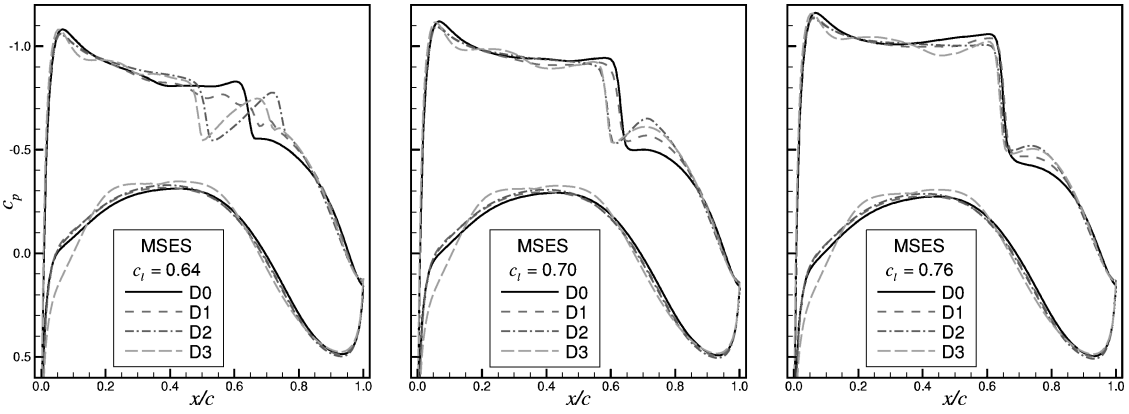

Fig. 9 Pressure coefficient distributions of the baseline D0 and three designs D1, D2, and D3, computed by MSES at $M = 0.76$.

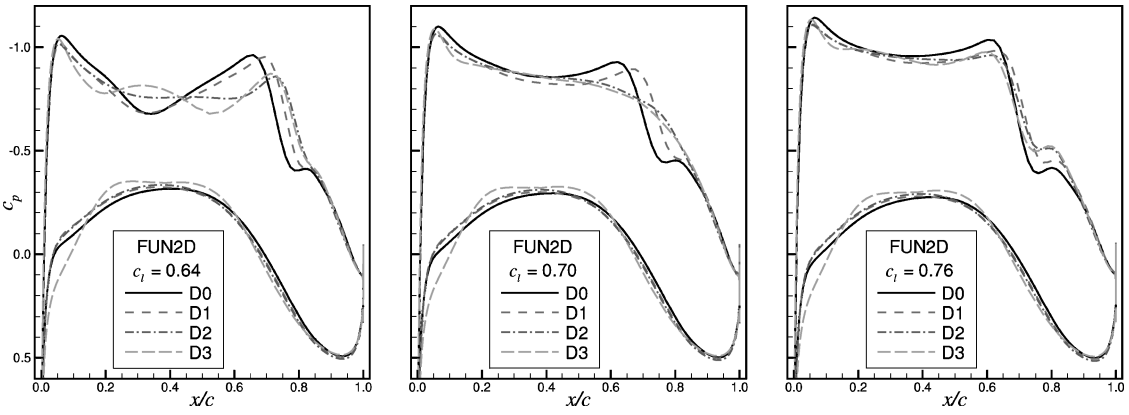

Fig. 10 Pressure coefficient distributions of the baseline D0 and three designs D1, D2, and D3, computed by FUN2D at $M = 0.76$.

the same. Although the expansion aft of the shock is significantly more pronounced for D2 than for D3, it does not completely explain the large performance penalty exhibited by D2 at $c_l = 0.70$; the performance of D3 is marginally better than that of D1 at this condition. Instead, one must consider the fact that pressure drag is a function of not only the pressure distribution but also the underlying surface shape upon which it acts; apparently, the shape of D2 is poorly suited in this regard.

Pressure distributions from FUN2D for the three designs at the three design conditions with $M = 0.76$, which are quite similar to those from OVERFLOW, are shown in Fig. 10. Here, the poor performance of D1 is easily ascertained as it exhibits significantly stronger shocks than those exhibited by D2 and D3 at all three conditions.

In evaluating the overall performance of the designs, including the performance at the fourth design condition of ($M = 0.70$, $c_l = 0.70$), which has yet to be addressed, we begin by considering the average drag of each of the designs. Table 1 shows the average drag coefficient at the four design conditions for D0, D1, D2, and D3 (airfoil D3s is discussed next) as computed by the three flow solvers. Numbers in the last row are the averages of the previous three rows. No matter which flow simulation code is used in the analysis, all three designs have lower average drag than D0 at the design conditions, while D3 has the lowest average drag among all of the candidate airfoil designs.

Additional detail on the global behavior of the designs is provided by considering drag-rise characteristics. Drag-rise curves from MSES at the three specified lift coefficients are shown in Fig. 11. The first point to note from these results is that the drag at ($M = 0.70$, $c_l = 0.70$) is substantially lower for D3 than for the other designs, providing an explanation for why the average drag

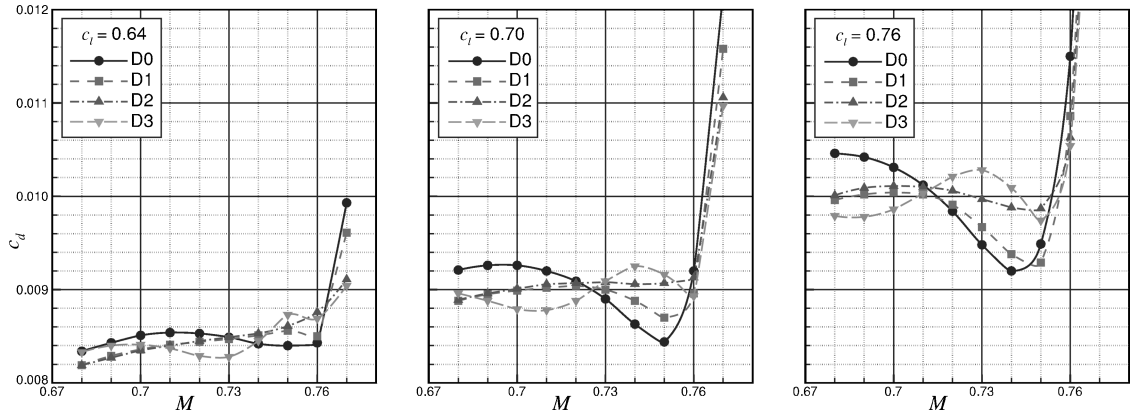

Fig. 11 Drag rise curves computed by MSES for the baseline D0 and three designs D1, D2, and D3.

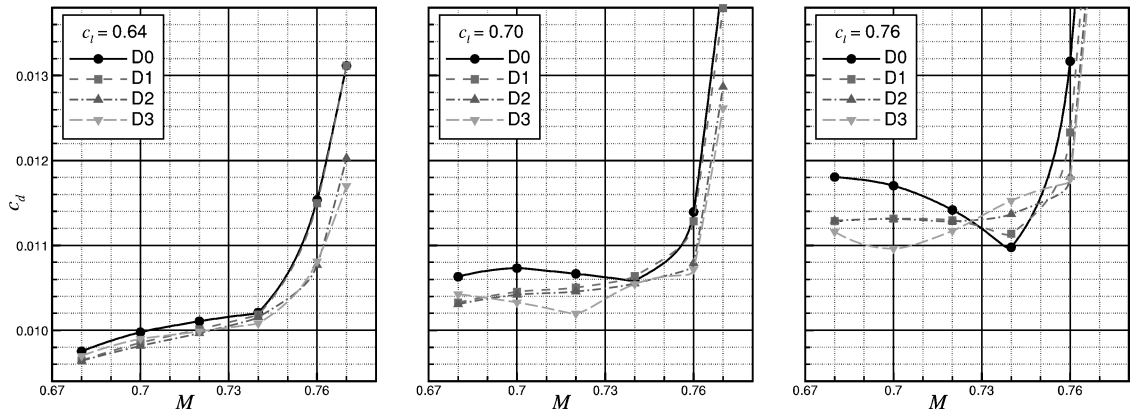

Fig. 12 Drag-rise curves computed by FUN2D for the baseline D0 and three designs D1, D2, and D3.

Table 1 Average drag coefficients at design conditions

Solver	D0	D1	D2	D3	D3s
MSES	0.00960	0.00933	0.00938	0.00924	0.00924
OVERFLOW	0.01158	0.01141	0.01096	0.01096	0.01096
FUN2D	0.01171	0.01139	0.01095	0.01091	0.01086
Average	0.01096	0.01071	0.01043	0.01037	0.01035

levels for D3 are so favorable even in MSES. Airfoils D1 and D2 also have significantly lower drag than the baseline at this condition. Of equal interest is that D0, D1, and D3 exhibit pronounced drag buckets in the vicinity of $M = 0.76$ when $c_l = 0.76$, with the extent of the drag bucket decreasing as the lift coefficient decreases. However, the drag bucket for D2 is quite mild at $c_l = 0.76$ and nonexistent at the lower lift coefficients. Even though D3 has no off-design performance degradation (i.e., the drag-rise curve does not have inverted V shape between the design Mach numbers) when analyzed by FUN2D, it exhibits severe off-design performance degradation at $M = 0.74$ for $c_l = 0.7$ when analyzed by MSES.

Drag-rise curves from OVERFLOW and FUN3D, which are quite similar, exhibit similar trends to those from MSES, but with some significant differences. The drag-rise curves, computed by FUN2D and shown in Fig. 12, indicate that the drag buckets of D0 and D1 are much less pronounced than those computed by MSES at $c_l = 0.76$ and nonexistent at lower lift coefficients. Moreover, drag buckets for D3 occur at Mach numbers well below $M = 0.76$. For D2, once again the drag-rise curves are quite smooth, with the drag-rise curve for $c_l = 0.76$ being nearly monotonic.

Of equal importance to drag-rise characteristics in assessing aircraft performance is the Mach variation of ML/D, which provides an indication of the range of the aircraft. Mach variations of ML/D computed by FUN2D at the three specified lift coefficients are shown in Fig. 13. Of particular interest here is that the ML/D curves for D3 are significantly less oscillatory than the drag-rise curves. Also worthy of note is that the ML/D values for D2 or D3 at the design cruise speed $M = 0.76$ are at a maximum or close to the maximum for each of the three lift coefficients, whereas for D0 or D1 the ML/D values drop precipitously after $M = 0.74$.

The preceding discussion leads to the consideration of robustness in the designs. In fact, a major impetus in developing the POM and POSSEM optimization methods has been to provide an optimizer capable of generating designs with robust performance. Unfortunately, definitions of robustness vary, from simple mathematical formulations based on the variance in the performance under the influence of small perturbations to the flight conditions, to more esoteric formulations involving aggregate performance over the range of flight conditions a vehicle is most likely to experience in operation. Moreover, it is unclear to the authors as to whether an appropriate measure of robustness exists for airfoil designs. As the nuances of the subject are well beyond the intent of this paper, for now we consider a robust airfoil to be one for which the performance variations with respect to changes in Mach number are not oscillatory, while also maximizing enhancements in performance across different analysis codes. Clearly, the first aspect of this definition as applied to the drag-rise curves favors D2, while the Mach variation of ML/D along with the second aspect of our definition of robustness favors D3.

Finally, we consider whether it is possible to use CFACS to smooth the curvature oscillations of D3 in a manner, which yields a better performing and more robust airfoil than D3. Plots of the upper surface curvature for such a smoothed variant, denoted as D3s, along with the pressure distribution at ($M = 0.76$, $c_l = 0.64$), are shown in Fig. 14. The surface curvature plot indicates that CFACS has smoothed out all curvature oscillations in D3, while also eliminating the sharp drop in curvature at the airfoil trailing edge. The pressure distribution indicates that the smoothed airfoil nearly eliminates

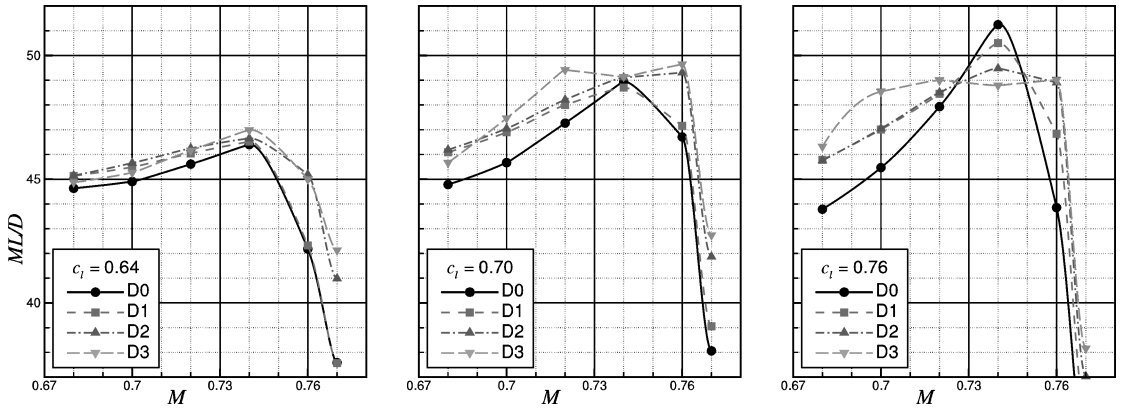

Fig. 13 Mach variation of ML/D computed by FUN2D for the baseline D0 and three designs D1, D2, and D3.

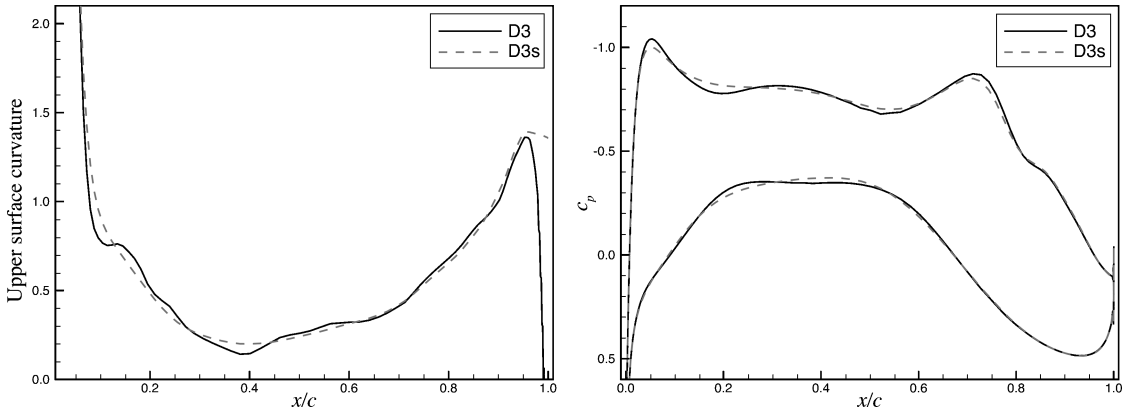

Fig. 14 Upper surface curvature and pressure coefficient distribution computed by FUN2D at (M = 0.76, c_l = 0.64) for D3 and its smoothed variant D3s.

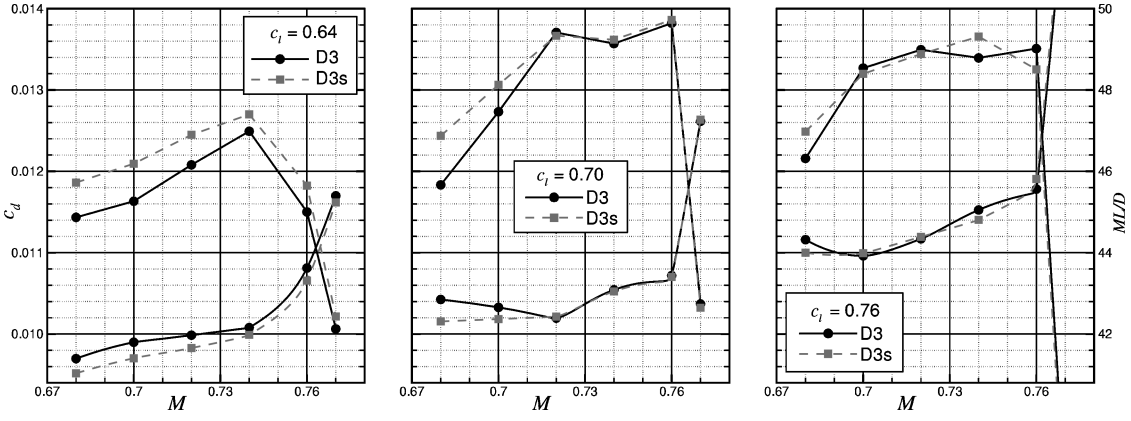

Fig. 15 Drag-rise curves (bottom curves) and Mach variation of ML/D (top curves) computed by FUN2D for D3 and its smoothed variant D3s at c_l = 0.64, 0.70, and 0.76.

inflections in the rooftop shape while reducing the shock strength. It also lowers the leading-edge suction peak, which tends to increase performance at lower Mach numbers but hurts performance at higher Mach numbers.

As shown in Table 1, the average drag computed by FUN2D for D3s is lower than that for D3, whereas the average drag values computed by MSES and OVERFLOW are unchanged. Drag-rise curves computed by FUN2D and the Mach variation of ML/D for D3 and D3s, shown in Fig. 15, indicate that D3s improves the performance at three of the four design points, with significant improvements at ($M = 0.70$, $c_l = 0.70$) and ($M = 0.76$, $c_l = 0.64$) and a significant penalty at ($M = 0.76$, $c_l = 0.76$). Moreover, both the drag and ML/D curves for D3s are much less inflectional than those for D3 with performance improvements at most of the off-design conditions. However, drag polar plots at $M = 0.76$ (not shown) indicate that the maximum L/D value for D3s is about 0.3 lower than that for D3.

In summary, POSSEM can generate smooth optimal airfoils with no off-design performance degradation, resolving two technically challenging problems encountered by multipoint airfoil shape optimization in a high-resolution design space. One could also allow POSSEM to put minor curvature oscillations on the airfoil surface for performance gains at high speed and high lift design condition(s) with minimum or no performance degradation at other flight conditions. Minor curvature oscillations of airfoils generated by POSSEM could be smoothed out by CFACS with no adverse effect on overall

performance of the airfoils. Moreover, optimal airfoils generated by POSSEM are as realistic as those generated by designers.

On the other hand, D3 with the lowest average drag at the design conditions is only about 6% better than D0, an airfoil quickly designed by using CDICS with MSES for flow simulation. This result really shows the power of the knowledge-based inverse design tool CDISC for capturing the main performance gain by using very simple inverse design rules for transonic aerodynamic shape design. Also, the marginal performance advantage of D3 over D2 shows that CDISC is a very powerful inverse design tool for subtle performance gains when it is appropriately used. In particular, smoothing the curvature of the airfoil designed for one flight condition with high lift and high speed is likely to promote performance at flight conditions of lower lift or lower speed, with minor performance loss at the design condition. This approach for inverse design leads to airfoil D2 with good performance over the range of flight conditions.

VI. Conclusions

Use of a low-resolution design space, as represented by a geometry model with a few shape parameters, is usually sufficient during the conceptual design of aerodynamic shapes. However, in a preliminary design environment it becomes necessary to use a high-resolution design space, as represented by a geometry model with as many as hundreds of shape parameters, particularly when searching for subtle performance gains from a fairly good baseline. Two technically challenging issues related to airfoil shape optimization in high-resolution design space are undesirable optimal airfoil shapes because of high-frequency components in the parametric airfoil model and off-design performance degradation because of lack of information on off-design performance within the optimization process. The use of smoothest shape modification along with simultaneous drag reduction at all of the design conditions during airfoil shape optimization provide a winning strategy to resolve these two issues. The airfoil optimization method using this strategy, called POSSEM, is thoroughly studied in this paper.

The smoothness measure for a shape modification $\Delta g(t)$ is the magnitude of the third derivative of $\Delta g(t)$. To get the last bit of performance gain, POSSEM might have to use shape modifications with relatively large third derivative bounds, resulting in an optimal airfoil with minor curvature oscillations. But minor curvature oscillations can easily be smoothed out by a spline-based airfoil curvature smoothing method, called CFACS, with no adverse effect on the overall performance of the optimal airfoil.

The utility of POSSEM is examined by conducting a design competition with the objective of improving a fairly well-designed baseline airfoil at four transonic flight conditions without incurring any off-design performance degradation. Three designs are generated independently, with the first two using a state-of-the-art inverse design method in conjunction with the two different flow solvers, respectively, and the third using POSSEM in conjunction with another flow solver. Pros and cons of all of the airfoil designs are documented along with in-depth analyses of the simulation results. Results from this study indicate that POSSEM largely resolves the two issues related to airfoil optimization in a high-resolution design space, generating an optimal airfoil with fairly smooth curvature that improves the performance of the baseline at multiple design conditions with no performance degradation at off-design conditions. Moreover, the performance of the airfoil generated by POSSEM is as competitive as or better than that of the airfoils generated by the inverse design methods no matter which flow solver is used in the analysis, implying that performance gains achieved by smooth global shape modifications are less code dependent.

To our knowledge, this study is the first successful attempt in generating realistic optimal airfoil designs through optimization in a high-resolution design space parameterized by a geometry model with over 200 shape design variables. The key to this success is the insistence on a smooth global shape modification in the formulation of POSSEM, which is necessary to ensure accurate linear Taylor approximations of the nonlinear aerodynamic coefficients as defined within Sobolev space.

Finally, we would like to point out that the smoothest shape modification and modified profile optimization strategies used in POSSEM are also applicable to three-dimensional aerodynamic shape optimization, provided that sensitivity information of the lift and drag coefficients with respect to the aerodynamic shape is available.

References

[1]Li, W., and Padula, S., "Using High Resolution Design Spaces for Aerodynamic Shape Optimization Under Uncertainty," NASA/TP-2004-213004, March 2004.

[2]Drela, M., "Pros and Cons of Airfoil Optimization," *Frontiers of Computational Fluid Dynamics 1998*, edited by D. A. Caughey and M. M. Hafez, World Scientific, Hackensack, NJ, 1998, pp. 363–382.

[3]Nemec, M., Zingg, D., and Pulliam, T., "Multi-Point and Multi-Objective Aerodynamic Shape Optimization," AIAA Paper 2002-5548, Sept. 2002.

[4]Jameson, A., and Vassberg, J., "Computational Fluid Dynamics for Aerodynamic Design: Its Current and Future Impact," AIAA Paper 2001-0538, Jan. 2001.

[5]Jameson, A., Shankaran, S., Martinelli, L., and Haimes, B., "Aerodynamic Shape Optimization of Complete Aircraft Configuration," AIAA Paper 2004-0533, Jan. 2004.

[6]Adams, R., *Sobolev Spaces*, Academic Press, New York, 1975.

[7]Li, W., Huyse, L., and Padula, S., "Robust Airfoil Optimization to Achieve Consistent Drag Reduction over a Range of Mach Numbers," *Structural Optimization*, Vol. 24, No. 1, 2002, pp. 38–50.

[8]Petropoulou, S., Pappou, T., Koubogiannis, D., and Freskos, G., "Multi-Point Airfoil Design Using a Continuous Adjoint Method," *Proceedings of the CEAS Aerospace Aerodynamics Research Conference*, Cambridge, U.K., June 2002, pp. 84.1–84.9.

[9]Padula, S., and Li, W., "Options for Robust Airfoil Optimization Under Uncertainty," AIAA Paper 2002-5602, Sept. 2002.

[10]Li, W., and Padula, S., "Performance Trades Study for Robust Airfoil Shape Optimization," AIAA Paper 2003-3790, June 2003.

[11]Campbell, R., "Efficient Viscous Design of Realistic Aircraft Configurations," AIAA Paper 98-2539, June 1998.

[12]Drela, M., "Newton Solution of Coupled Viscous/Inviscid Multielement Airfoil Flows," AIAA Paper 90-1470, June 1990.

[13]Buning, P. G., Jespersen, D. C., Pulliam, T. H., Klopfer, G. H., Chan, W. M., Slotnick, J. P., Krist, S. E., and Renze, K. J., *OVERFLOW User's Manual*, ver. 1.8, NASA Langley Research Center, Hampton, VA, 1998.

[14]Anderson, W., and Bonhaus, D., "An Implicit Upwind Algorithm for Computing Turbulent Flows on Unstructured Grids," *Computers and Fluids*, Vol. 23, No. 1, 1994, pp. 1–21.

[15]Anderson, W., and Bonhaus, D., "Aerodynamic Design on Unstructured Grids for Turbulent Flows," NASA Technical Memorandum 112867, June 1997.

[16]Li, W., and Krist, S., "Spline-Based Airfoil Curvature Smoothing and Its Applications," *Journal of Aircraft*, Vol. 42, No. 4, 2005, pp. 1065–1074.